NeuroImage: Clinical 15 (2017) 581–586

Contents lists available at ScienceDirect

NeuroImage: Clinical

journal homepage: www.elsevier.com/locate/ynicl

APPswe/PS1dE9 mice with cortical amyloid pathology show a reduced NAA/Cr ratio without apparent brain atrophy: A MRS and MRI study

Angela Kuhla[a,*], Claire Rühlmann[a], Tobias Lindner[b], Stefan Polei[b], Stefan Hadlich[c], Bernd J. Krause[d], Brigitte Vollmar[a], Stefan J. Teipel[e]

[a] Institute for Experimental Surgery, Rostock University Medical Center, Rostock, Germany
[b] Core Facility Multimodal Small Animal Imaging, Rostock University Medical Center, Rostock, Germany
[c] Institute of Diagnostic Radiology and Neuroradiology, University Medicine Greifswald, Greifswald, Germany
[d] Department of Nuclear Medicine, Rostock University Medical Center, Rostock, Germany
[e] German Center for Neurodegenerative Diseases (DZNE) - Rostock/Greifswald, Rostock, Germany, Department of Psychosomatic Medicine, University of Rostock, Rostock, Germany

ARTICLE INFO

Keywords:
APPswe/PS1dE9 mice
Neuronal loss
Aβ-plaques
NAA/Cr ratio
Brain atrophy

ABSTRACT

Transgenic animal models of Aβ pathology provide mechanistic insight into some aspects of Alzheimer disease (AD) pathology related to Aβ accumulation. Quantitative neuroimaging is a possible aid to improve translation of mechanistic findings in transgenic models to human end phenotypes of brain morphology or function. Therefore, we combined MRI-based morphometry, MRS-based NAA-assessment and quantitative histology of neurons and amyloid plaque load in the APPswe/PS1dE9 mouse model to determine the interrelationship between morphological changes, changes in neuron numbers and amyloid plaque load with reductions of NAA levels as marker of neuronal functional viability. The APPswe/PS1dE9 mouse showed an increase of Aβ plaques, loss of neurons and an impairment of NAA/Cr ratio, which however was not accompanied with brain atrophy. As brain atrophy is one main characteristic in human AD, conclusions from murine to human AD pathology should be drawn with caution.

1. Introduction

The deposition of β-amyloid (Aβ) is considered one of the initial events in the pathogenesis of Alzheimer's disease (AD) (Braak and Braak, 1991), and most likely begins years before the onset of detectable cognitive symptoms in familial (Bateman et al., 2012) as well as sporadic forms of AD (Skoog et al., 2003). In the classical model, initial Aβ accumulation is followed by gradual progression of neurodegeneration and subsequent cognitive decline (Jack et al., 2010). Transgenic animal models of Aβ pathology provide mechanistic insight into some aspects of AD pathology related to Aβ accumulation, but transfer of findings to the AD phenotype in humans is limited (Foley et al., 2015). Using quantitative neuroimaging is a possible aid to improve translation of mechanistic findings in transgenic models to human end phenotypes of brain morphology or function (Teipel et al., 2011). Brain morphometry based on high resolution MRI is considered a proxy of neuronal loss in humans (Bobinski et al., 2000). Proton magnetic resonance spectroscopy (^{1}H-MRS) is an in-vivo technique to analyze neuronal functional viability in transgenic animal models (Mlynárik et al., 2012) and human studies (Arora and Bhagat, 2016). Each observable metabolite can potentially serve as a marker being representative for pathological processes at a molecular or cellular level. *N*-acetylaspartate (NAA) is considered to reflect neuronal mitochondrial function (Clark, 1998; Moffett et al., 2007). So, reduced NAA levels are found in AD patients in correlation to brain pathology and disease progression (Ross et al., 1998). Although they appear to be partly independent from regional atrophy (Schuff et al., 1997), diminished NAA-levels may potentially serve as functional markers of intervention effects (Paslakis et al., 2014). NAA reductions have been described in a wide range of transgenic models of Aβ pathology (Chen et al., 2012; Mlynárik et al., 2012).

A common AD model is the APPswe/PS1dE9 mouse that is characterized by an early-onset age-related increase in Aβ-levels with Aβ depositions starting at 4–6 months of age and morphological alterations (Garcia-Alloza et al., 2006). In a longitudinal study using APPswe/PS1 (M146L) mice from 2.5 to 9 months of age, Lau et al. (2008) observed volumetric reductions in these animals, although no general brain atrophy was found. The authors stated that most of the anatomical differences appeared to result from a developmental, rather than a degenerative process (Lau et al., 2008). Richner et al. (2009) reported a

* Corresponding author at: Institute for Experimental Surgery, Rostock University Medical Center, Schillingallee 69a, 18057 Rostock, Germany.
E-mail address: angela.kuhla@uni-rostock.de (A. Kuhla).

http://dx.doi.org/10.1016/j.nicl.2017.06.009
Received 22 February 2017; Received in revised form 7 April 2017; Accepted 8 June 2017
Available online 09 June 2017

significantly lower number of neurons in the striatum of 12-month old APPswe/PS1dE9 mice compared with 12-month old wild type and 6-month-old transgenic mice. In line with this, studies of Chen et al. (2012) and Marjanska et al. (2005) demonstrated in APPswe/PS1dE9 and APPswe/PS1 (M146L) mice, respectively, at ages > 8 months a reduced NAA levels in ^{1}H-MRS, indicating neuronal loss.

Here, we combined MRI-based morphometry, MRS-based NAA-assessment and histological analysis of neuron and glial cell numbers and amyloid plaque load in the APPswe/PS1dE9 mouse model to comprehensively assess interaction between histological and neuroimaging markers of neuronal loss, neuronal function, and brain atrophy. We hypothesized that we would find more pronounced alterations of NAA as a functional marker instead of volumetric changes, in the APPswe/PS1dE9 animals at the age of 12 months compared with age-matched wildtype controls. These data would support the interpretation of MRS changes in human studies and might serve as basis for the future use of MRS-based NAA assessment in preclinical intervention trials.

2. Material & methods

2.1. Animals

Double transgenic female APPswe/PS1dE9 (tg) mice on the genetic background of C57BL/6J and C3H/HeJ (MMRRC, mutant mouse resource & research centers, n = 10) at the age of 12 months were used for this study. These mice co-express the PS1d9 mutant form of PS1 and a chimeric mouse-human APP_{695} with mutations $K_{594}N$ and $M_{595}L$ driven by the mouse prion protein promotor. For controls, wild type (wt) age-matched littermates (n = 9) were used. All mice were bred at the host institution with a permission of MMRCC. All mice housed in standard cages in a temperature-controlled room (22 °C ± 2 °C) on a 12 h light/dark cycle (light on at 06:00 a.m.) with free access to standard pellet food and water under specified pathogen free (SPF) conditions. The experimental protocol was approved by the local Animal Research Committee (Landesamt für Landwirtschaft, Lebensmittelsicherheit und Fischerei (LALLF) of the state Mecklenburg-Western Pomerania (LALLF M-V/TSD/7221.3-1.1-002/14) and all animals received humane care according to the German legislation on protection of animals and the Guide for the Care and Use of Laboratory Animals (NIH publication 86–23 revised 1985).

2.2. In vivo morphologic and spectroscopic MRI

All mice were anesthetized with 1–3% isoflurane in 100% O_2. The mice heads were placed with the animal's incisors secured over a bite bar and ophthalmic ointment was applied to the eyes. Anesthetized mice were scanned in a 7 T small animal MRI (Bruker Biospec 70/30, gradient inset: BGA-12S, 440 mT/m gradient strength, Paravision 6 interface) in combination with a cryogenic transmit/receive RF surface coil (Bruker ^{1}H MRI CryoProbe two element array kit for mice) specially designed for mouse brain measurements. Animal welfare was ensured by employing a water driven warming mat as well as constant respiration and core body temperature monitoring.

The imaging protocol included a morphological, respiration triggered, transversal T2-weighted (T2w) RARE (Rapid Acquisition with Relaxation Enhancement) sequence with following parameters: TE/TR: 39/2200 ms; FoV: approx. 13 mm × 17 mm; matrix: 200 pix × 260 pix; voxel size: 0.065 mm × 0.065 mm × 0.5 mm, approx. 18 slices. In addition, T2w images with similar resolution in the sagittal and coronal plane were acquired for magnetic resonance spectroscopy (^{1}H–MRS) voxel placement. Respiration triggered ^{1}H–MRS was carried out by means of the Stimulated Echo Acquisition Method (STEAM) with outer volume suppression and a voxel volume of approximately 10 mm^3 (placed in the cortex and hippocampus, see Fig. 3A). The parameters used were: acquisition bandwidth: 4.9 kHz; TE/TR: 135/1500 ms; mixing time 11,75 ms, 512 averages; acquisition time: 13 min. Each free induction decay was recorded with 2048 complex points. The water signal was suppressed using the variable pulse power and optimized relaxation delays (VAPOR, Tkác et al., 1999) scheme. Based on B_0-field map measurements, the linewidth/spectral resolution was optimized by adjustments of first- and (if necessary) second-order shims, resulting in an average full width half maximum linewidth of the unsuppressed water peak between 10 Hz and 25 Hz.

2.3. Analysis of MRS data

^{1}H–MRS data were evaluated using the jMRUI software package 5.2 (Stefan et al., 2010; Naressi et al., 2001). In order to compute metabolite ratios (NAA/Cr) ^{1}H–MRS spectra were fitted using the Hankel Lanczos singular value decomposition (HLSVD) algorithm (Pijnappel et al., 1992). This space-state based method allows for efficient spectra analysis with very limited user interaction (black-box method). Prior to the fit, the spectra were corrected for phase-errors (0th order) and temporal shifts (group delay) of the free induction decay. For the fit of metabolite peaks we identified the amount of component peaks (typically 6) which should be contained in the spectral data. Metabolite ratios were calculated based on area under the correspondent fitted curves for *N*-acetylaspartate (NAA 2.0 ppm), creatine (Cr 3.0 ppm) and choline (Cho 3.2 ppm).

2.4. Morphometric analysis

Voxel-based morphometric analysis of the T2-weighted RARE sequences was implemented with Matlab 8.1.0.604 (MathWorks, USA) through Statistical Parametric Mapping (Friston et al., 1995a; Friston et al., 1995b) (SPM 8, Wellcome Department of Imaging Neuroscience, London; available at http://www.fil.ion.ucl.ac.uk/spm) and SPMMouse (Wolfson Brain Imaging Centre, University of Cambridge, UK), a Matlab-based modification of SPM5 and SPM8, available at (http://www.wbic.cam.ac.uk/~sjs80/spmmouse.html) (Sawiak et al., 2009). SPMMouse implements grey matter, white matter and CSF space probability maps from a high-resolution sequence that is in affine co-registration with a publicly-available digital C57BL/6J mouse atlas (Ma et al., 2005). The processing of our data followed four subsequent steps.

In the *first step*, the T2-weighted RARE sequences were coregistered to their common mean in native space using 6-parameter rigid body transformation. The aligned scans were averaged, and the ensuing mean image was segmented into grey matter, white matter and CSF maps. The SPM segmentation employs a mixture model cluster analysis (after correcting for non-uniformity in image intensity using light regularization) to identify voxel intensities that match particular tissue types combined with a priori probabilistic knowledge of the spatial distribution of tissues derived from grey and white matter and CSF prior probability images (priors) (Ashburner and Friston, 1997). Prior probability images were derived from the tissue maps implemented in SPMMouse that are in co-registration with a digital mouse atlas (Sawiak et al., 2009).

The resulting grey matter, white matter and CSF maps were summed and binarized to obtain a binary brain mask that was used in the *second step* to mask the segmentation of the individual realigned T2-weighted RARE scans using the segmentation procedure described above using light regularization to account for signal inhomogeneity in the scans.

The resulting grey matter segments of each brain scan in native space were then high-dimensionally registered to create a common group specific reference template using DARTEL (Ashburner, 2007). This group specific template served to accommodate potential gross differences in brain morphology between the APPswe/PS1dE9 (tg) and the wildtype (wt) mice, as well as between the C57BL/6J and C3H/HeJ background of our animals and the C57BL6 reference. Individual flow-fields resulting from the DARTEL registration to the reference template for each scan were used to warp the GM segments and voxel-values

were modulated for volumetric changes introduced by the high-dimensional normalization, such that the total amount of GM volume present before warping was preserved. Finally, the normalized maps were smoothed with a 0.5 mm full width at half maximum isotropic Gaussian kernel before subsequent statistical analysis.

2.5. Tissue sampling

All mice were sacrificed after experimental procedures according to approved animal experimental protocol and brain tissue was harvested for histopathological analysis.

2.6. Histopathology

For immunohistochemical analysis, brain tissue was fixed in 4% phosphate-buffered formalin for 5–6 weeks and subsequently embedded in paraffin. From the paraffin-embedded tissue blocks, 4 µm thin sections were put on X-tra Adhesive Precleaned Micro Slides (Leica) and exposed to a mouse monoclonal anti-Aβ antibody (clone 6E10; 1:1000, BioLegend (previous Covance); as described by Sudduth et al., 2013), rabbit polyclonal anti-GFAP antibody (1:100, abcam; as described by Lu et al., 2010) and rabbit polyclonal anti-NeuN antibody (1:1000, abcam, as described by Park et al., 2016). For the development DAB chromogen Universal LSAB® kits (System-HRP; DakoCytomation, Dako) were used according to the manufacturer's instructions. The sections were counterstained with hemalaun and analyzed with a light microscope (Olympus BX51). Images were acquired with a Color View II FW camera (Color View). Within the hippocampus (n = 4 of each mouse strain, n = 25 of visual fields) and cortex (n = 4 of each mouse strain, n = 40 of visual fields), the number of anti-Aβ positive plaques, anti-GFAP and anti-NeuN positive cells were counted and given as number per mm^2.

2.7. Statistical analysis

Statistical differences in scalar measures from MRS and quantitative histology were determined using ANOVA on ranks (Mann-Whitney Rank Sum test). Data were considered significant if $p < 0.05$. Statistical analysis was performed using the SigmaStat software package (Jandel Scientific). For voxel-wise statistical analysis, we employed the general linear model on a voxel basis, where we assessed the effect of genotype on grey matter density. Smoothed T2 relaxation times and grey matter maps were masked for tissue outside of the grey matter using the segmented grey matter map from the group-specific brain template. Results were thresholded at a liberal level of $p < 0.01$, uncorrected for multiple comparisons, and an extent threshold of 5 contiguous voxels was applied. We used a liberal p-value due to our primary hypothesis that MRS-based NAA measures would be more sensitive than morphometric measures for genotype induced changes. Therefore, we used a liberal p-value to reduce the risk of a false negative finding, i.e. that we do not detect a morphometric effect although it is present, and thus overestimate the effect of NAA in comparison with morphometry.

3. Results

3.1. Morphometry

Even at a liberal p-value of $p < 0.01$ at 17 df we found only a few scattered clusters of reduced grey matter volume in tg animals compared with wt controls throughout several brain regions, including caudate, hippocampus and cerebellum (Fig. 1). The opposite contrast (i.e. increased grey matter volume in tg vs. wt animals) revealed scattered cluster in other brain regions but to a similar extent (data not shown). The effects in both directions did not survive a p-value of $p < 0.05$ using false discovery rate (FDR) correction (Genovese et al.,

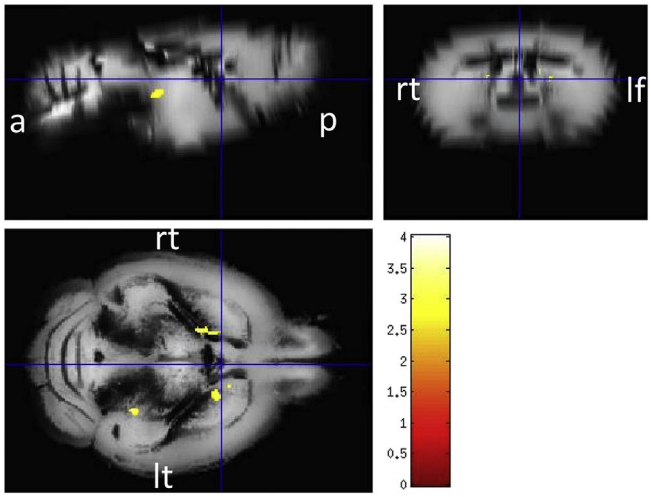

Fig. 1. Significant reductions of grey matter volumes in transgenic APPswe/PS1dE9 (tg) mice compared to wild type (wt) mice indicated by the colored regions where the colon intensity corresponds to the voxel-wise *t*-value (see color bar in the right). Cluster extension set at ≥ 5 contiguous voxels passing the significance threshold of $p < 0.01$, uncorrected. Effects are projected on the group-specific averaged anatomical image in standard space representing the template brain. The right side of the image corresponds to the right side of the brain (a: anterior, p: posterior, rt.: right, lt: left). (For interpretation of the references to color in this figure legend, the reader is referred to the web version of this article.)

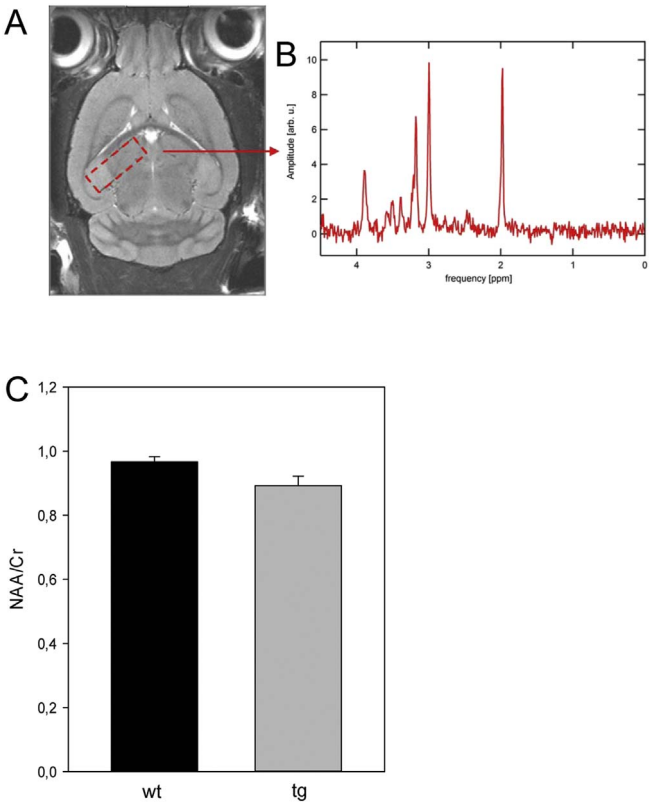

Fig. 2. (A): Transversal T2 weighted MRI image including position of the spectroscopy voxel (red dashed box). (B) MRS spectrum as derived from the voxel of interest shown in A. Two prominent metabolites, e.g. *N*-acetylaspartate (NAA resonates at 2.0 ppm) and creatine (Cr at 3.0 ppm) from a tg (APPswe/PS1dE9) mouse are evident and were further evaluated. (C). Diagram of the NAA/Cr ratio in wild type (wt) and transgenic APPswe/PS1dE9 (tg) mice. Values are given as mean ± SEM. (For interpretation of the references to color in this figure legend, the reader is referred to the web version of this article.)

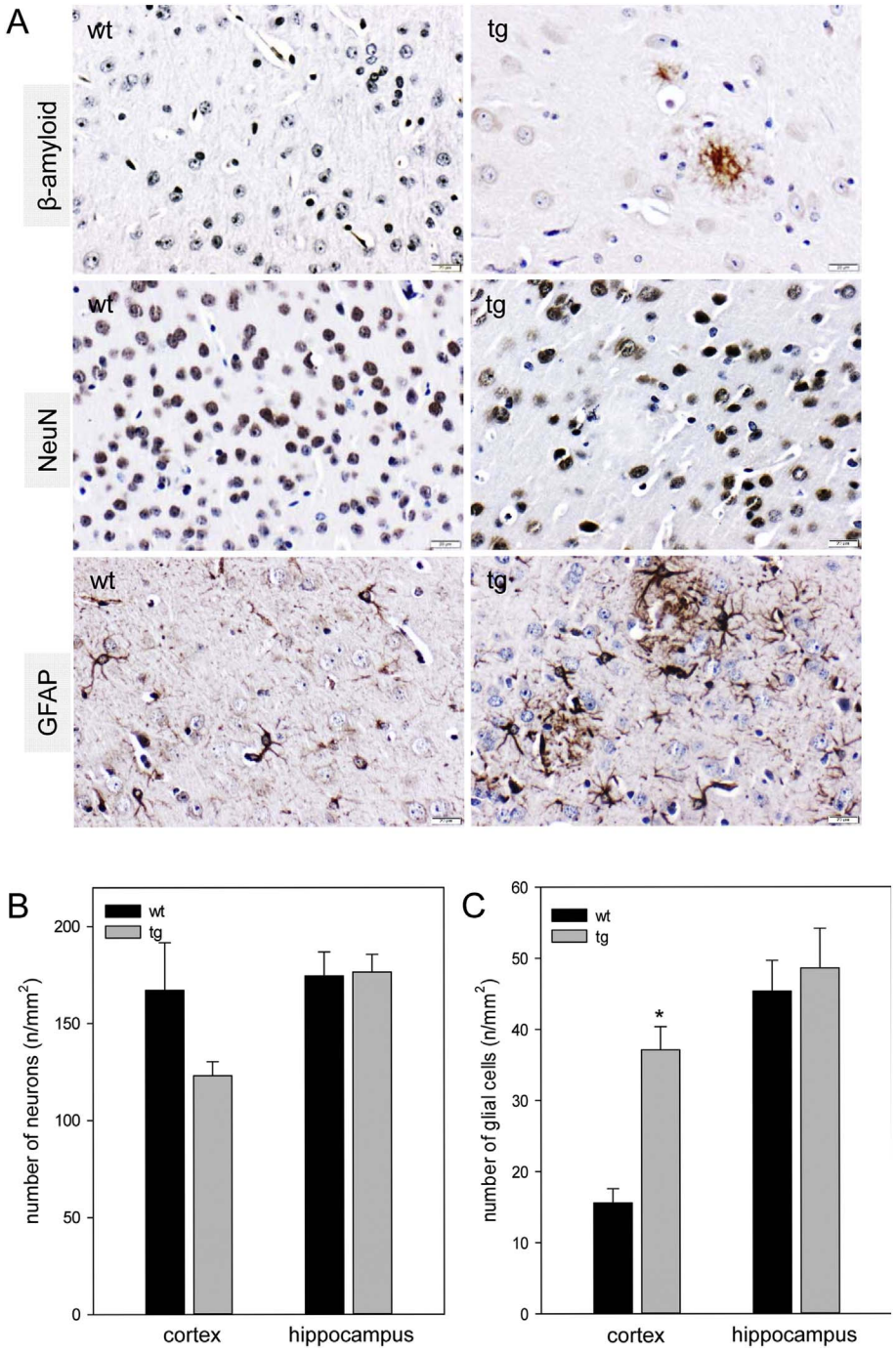

Fig. 3. (A) Representative immunohistochemical images (scale bar 20 μm) of β-amyloid-plaques (upper panels), of NeuN positive neurons (middle panels) and of GFAP positive glial cells (lower panels) in the entorhinal cortex of wild type (wt, left panels) and of transgenic (tg, right panels) mouse. (B and C) Quantitative analysis of the number of NeuN positive neurons (B) and of GFAP positive glial cells (C) per mm^2 in the cortex and in the hippocampus of wild type (wt) and of transgenic APPswe/PS1dE9 (tg) mice. Values are given as mean ± SEM; ANOVA on ranks (Mann-Whitney Rank Sum test): * $p < 0.05$ vs. wt.

2002), suggesting that the majority of findings represents false positives.

3.2. MR spectroscopy

In Fig. 2A a transversal T2 weighted MRI image including position of the spectroscopy voxel (red dashed box) is shown. An example of a MRS spectrum as derived from the voxel of interest is shown in Fig. 2B. Two prominent metabolites, i.e. *N*-acetylaspartate (NAA resonates at 2.0 ppm) and creatine (Cr at 3.0 ppm) from a tg mouse are evident and were further evaluated across all animals. MR spectroscopy revealed a moderate and marginally significant ($p = 0.052$) difference of up to 10% of NAA/Cr ratio in wt mice when compared to tg mice of the same age (NAA/Cr ratio wt 0.97 ± 0.02, tg 0.89 ± 0.03).

3.3. Immunohistochemistry

In general, brain tissue of wt mice (Fig. 3A, upper left panel) were free of anti-Aβ positive plaques, while in tg mice (Fig. 3A, upper right panel) abundant anti-Aβ positive plaques were found throughout brain tissue. In the hippocampal and cortical area, respectively, the number of plaques was either 2.9 ± 0.11 (hippocampus) or 4.4 ± 0.32 (cortex) per mm^2 whereby the plaque area per mm^2 was either 1% ± 0.1 (hippocampus) or 2% ± 0.8 (cortex) in tg mice. In addition, tg mice revealed an up to 27% decrease of the number of NeuN-positive neuronal cells in the cortex (Fig. 3A, middle right panel and 3B) when compared to wt mice (Fig. 3A, middle left panel and 3B), while in the hippocampal area no difference between the mice strains concerning the NeuN positive cells was observed. The analysis of GFAP positive cells demonstrated that tg mice are characterized by a raised

cortical gliosis ($p = 0.002$; at 5 df, Fig. 3A, lower right panel) as indicated by an up to 2.5-fold increase of GFAP positive glial cells when compared to wt mice (Fig. 3C). Again, there was no change of GFAP positive cells in the hippocampus in response to the transgenic genotype when compared to wt mice (Fig. 3C).

4. Discussion

In this work, we combined MRI-based morphometry, MRS-based NAA-assessment and histological assessment of neurons, glial cells and amyloid plaque load in the APPswe/PS1dE9 mouse model whereby the brain was not sectioned serially. For this study, we used voxel-based morphometry of high resolution anatomical MRI scans to determine a pattern of volume reduction, in analogy to brain atrophy in AD. MRI is extensively used for the diagnosis of mild cognitive impairment and AD, thereby the detection of a medial temporal atrophy is already considered as a biomarker for AD (Craig-Schapiro et al., 2009; Johnson et al., 2012). However, although our tg mouse model has demonstrated many of the cognitive Savonenko et al., 2005; Minkeviciene et al., 2008) and neuropathological features of AD, including senile plaques (present study), these mice revealed no atrophic changes in comparison to wt littermates. This is in line with a longitudinal study in APPswe/PS1 (M146L) mice of Lau et al. (2008) who reported admittedly volumetric reduction but no general brain atrophy. The authors concluded that this phenomenon appeared as a result from a developmental rather than a degenerative process (Lau et al., 2008). However, a former study from Delatour et al. (2006) using APPswe/PS1 (M146L) mice of advanced age (24 months) reported a moderate global brain atrophy. This atrophy had the focus in midbrain areas and not, as excepted from AD, at hippocampal levels. Although all these studies used a different AD mouse model, it can be assumed that likewise to the 9 months old APPswe/PS1 (M146L) mice (Lau et al., 2008) also the 12 months APPswe/PS1dE9 mice (present study) were too young to exhibit any brain atrophy. However, we found reductions of cortical neuron numbers, which is in line with previous findings in APPswe/PS1dE9 mice showing reduced numbers of neurons in the striatum (Richner et al., 2009). This cortical neuron loss, however, was not reflected in the MRI based grey matter morphometry findings. In summary, the discrepant literature on MRI volumetric changes might strongly be dependent on the age and on the mouse strains, being used (Kärkkäinen et al., 2015). An alternative explanation for the discrepancy between missing atrophy despite neuronal loss may be the already described increase of glial cells (Manaye et al., 2007) in the corresponding brain regions that different to human AD may mask the effect of neuron loss on grey matter volume estimates from MRI. Indeed, recent evidence from a prospective intervention study in wt mice suggest that both hippocampal neuroneogenesis induced by physical exercise and glial cell numbers contribute to MRI based hippocampus volume estimates (Biedermann et al., 2016). Unfortunately, we were not able to correlate MRI and histology findings on a regional basis since we performed the histology analysis post hoc when we found no atrophy effects (so that sections could no more be matched to the MRI regions). A prospective study with parallel sampling of brain MRI and tissue sections would be valuable to provide quantitative evidence on the relative contribution of neuron and glial cells numbers on estimates of brain volume in MRI. To draw conclusions on the current study it should kept in mind that the estimation for the hippocampal volume might be less accurate than that of the neocortex when using 2D instead of isotropic 3D sequences.

In human studies, the major contributor to atrophy is thought to be dendritic and neuronal loss. In line with this, human studies of regional (e.g. hippocampal) MRI volumes show that these are closely related to neuronal counts at autopsy (Bobinski et al., 2000; Gosche et al., 2002; Jack et al., 2002). Our data suggest that this is not the case in APPswe/PS1dE9 mice. In addition, the distribution of neuron loss sparing the hippocampus area in the APPswe/PS1dE9 mice contrasts with the characteristic pattern of neuronal loss in AD (Price et al., 2001).

In agreement with the finding of neuronal loss, the neurochemical profile was changed as indicated by a moderate ($p = 0.052$) decrease of the NAA to Cr ratio in tg mice when compared with wt littermates. In line with this finding, Chen et al. (2012) reported that these tg mice already at age of 8 months revealed a decrease of NAA to Cr ratio. Another group found similar reductions in the levels of NAA compared with total Cr levels measured by ^{1}H–MRS, but in APPswe/PS1 (M146L) mice, which were found further reduced with advancing age (Marjanska et al., 2005). The authors stated that this age-dependent neurochemical changes observed in APPswe/PS1 (M146L) mice were in agreement with results obtained from in vivo human MRS studies (Marjanska et al., 2005). Therefore, they assumed that AD mouse model could substantially contribute to the understanding of AD and accelerate drug discovery.

Our data further qualify this statement: MRS changes may mirror a key feature of AD like decline of neuronal viability, but measures of atrophy are not useful to translate and back-translate findings in this mouse model and human studies. As observed here, the APPswe/PS1dE9 mice are characterized by a marked increase of inflammatory GFAP-positive cells. There is a great line of evidence that microglia activation with CD11b immunoreactivity is induced by Aβ (Gallagher et al., 2013). Consistent with this assumption, APPswe/PS1dE9 mice of the current study presented high numbers of GFAP positive microglia and a high Aβ load. Further, it is reported that brain atrophy in amyloid producing mice appears to be masked by volume increase due to amyloid accumulation and especially accompanying astrogliosis (Kärkkäinen et al., 2015).

4.1. Conclusions

In summary, APPswe/PS1dE9 mice as a model of AD showed an increase of Aβ plaques, a loss of neurons and an impairment of NAA/Cr ratio, which however was not accompanied with brain atrophy. As brain atrophy is one main characteristic in human AD conclusions from murine to human AD pathology should be drawn with caution.

Acknowledgements

This study was supported by a grant from the German Research Foundation (DFG, Bonn-Bad Godesberg, Germany; KU 3280/1-1) and by the Marie-Curie Innovative Training Network BBDiag (EU-Horizon2020 Project ID: 721281). The authors thank the Medical Faculty of the Rostock University Medical Center for the financial support of the imaging consortium and gratefully acknowledge the technical support of Romina Rauer and Anne Möller.

References

Arora, A., Bhagat, N., 2016. Insight into the molecular imaging of Alzheimer's disease. Int. J. Biomed. Imaging. 2016, 7462014.
Ashburner, J., 2007. A fast diffeomorphic image registration algorithm. NeuroImage 38, 95–113.
Ashburner, J., Friston, K., 1997. Multimodal image coregistration and partitioning–a unified framework. NeuroImage 6, 209–217.
Bateman, R.J., Xiong, C., Benzinger, T.L., Fagan, A.M., Goate, A., Fox, N.C., Marcus, D.S., Cairns, N.J., Xie, X., Blazey, T.M., Holtzman, D.M., Santacruz, A., Buckles, V., Oliver, A., Moulder, K., Aisen, P.S., Ghetti, B., Klunk, W.E., McDade, E., Martins, R.N., Masters, C.L., Mayeux, R., Ringman, J.M., Rossor, M.N., Schofield, P.R., Sperling, R.A., Salloway, S., Morris, J.C., 2012. Dominantly inherited Alzheimer network. Clinical and biomarker changes in dominantly inherited Alzheimer's disease. N. Engl. J. Med. 367, 795–804.
Biedermann, S.V., Fuss, J., Steinle, J., Auer, M.K., Dormann, C., Falfán-Melgoza, C., Ende, G., Gass, P., Weber-Fahr, W., 2016. The hippocampus and exercise: histological correlates of MR-detected volume changes. Brain Struct. Funct. 221, 1353–1363.
Bobinski, M., de Leon, M.J., Wegiel, J., Desanti, S., Convit, A., Saint Louis, L.A., Rusinek, H., Wisniewski, H.M., 2000. The histological validation of post mortem magnetic resonance imaging-determined hippocampal volume in Alzheimer's disease. Neuroscience 95, 721–725.
Braak, H., Braak, E., 1991. Neuropathological stageing of Alzheimer-related changes. Acta Neuropathol. 82, 239–259.
Chen, S.Q., Cai, Q., Shen, Y.Y., Wang, P.J., Teng, G.J., Zhang, W., Zang, F.C., 2012. Age-

related changes in brain metabolites and cognitive function in APP/PS1 transgenic mice. Behav. Brain Res. 235, 1–6.
Clark, J.B., 1998. *N*-acetyl aspartate: a marker for neuronal loss or mitochondrial dysfunction. Dev. Neurosci. 20, 271–276.
Craig-Schapiro, R., Fagan, A.M., Holtzman, D.M., 2009. Biomarkers of Alzheimer's disease. Neurobiol. Dis. 35, 128–140.
Delatour, B., Guégan, M., Volk, A., Dhenain, M., 2006. In vivo MRI and histological evaluation of brain atrophy in APP/PS1 transgenic mice. Neurobiol. Aging 27, 835–847.
Foley, A.M., Ammar, Z.M., Lee, R.H., Mitchell, C.S., 2015. Systematic review of the relationship between amyloid-β levels and measures of transgenic mouse cognitive deficit in Alzheimer's disease. J. Alzheimers Dis. 44, 787–795.
Friston, K., Ashburner, J., Frith, C.D., Poline, J.B., Heather, J.D., Frackowiak, R.S.J., 1995a. Spatial registration and normalization of images. Hum. Brain Mapp. 2, 165–189.
Friston, K., Holmes, A.P., Worsley, K., Poline, J.B., Frith, C.D., Frackowiak, R.S.J., 1995b. Statistical parametric maps in functional imaging: a general linear approach. Hum. Brain Mapp. 2, 189–210.
Gallagher, J.J., Minogue, A.M., Lynch, M.A., 2013. Impaired performance of female APP/PS1 mice in the Morris water maze is coupled with increased Aβ accumulation and microglial activation. Neurodegener. Dis. 11, 33–41.
Garcia-Alloza, M., Robbins, E.M., Zhang-Nunes, S.X., Purcell, S.M., Betensky, R.A., Raju, S., Prada, C., Greenberg, S.M., Bacskai, B.J., Frosch, M.P., 2006. Characterization of amyloid deposition in the APPswe/PS1dE9 mouse model of Alzheimer disease. Neurobiol. Dis. 24, 516–524.
Genovese, C.R., Lazar, N.A., Nichols, T., 2002. Thresholding of statistical maps in functional neuroimaging using the false discovery rate. NeuroImage 15, 870–878.
Gosche, K.M., Mortimer, J.A., Smith, C.D., Markesbery, W.R., Snowdon, D.A., 2002. Hippocampal volume as an index of Alzheimer neuropathology: findings from the Nun Study. Neurology 58, 1476–1482.
Jack Jr., C.R., Dickson, D.W., Parisi, J.E., Xu, Y.C., Cha, R.H., O'Brien, P.C., Edland, S.D., Smith, G.E., Boeve, B.F., Tangalos, E.G., Kokmen, E., Petersen, R.C., 2002. Antemortem MRI findings correlate with hippocampal neuropathology in typical aging and dementia. Neurology 58, 750–757.
Jack Jr., C.R., Knopman, D.S., Jagust, W.J., Shaw, L.M., Aisen, P.S., Weiner, M.W., Petersen, R.C., Trojanowski, J.Q., 2010. Hypothetical model of dynamic biomarkers of the Alzheimer's pathological cascade. Lancet Neurol. 9, 119–128.
Johnson, K.A., Fox, N.C., Sperling, R.A., Klunk, W.E., 2012. Brain imaging in Alzheimer disease. Cold Spring Harb. Perspect. Med. 2, a006213.
Kärkkäinen, E., Lahtinen, H.M., Närväinen, J., Gröhn, O., Tanila, H., 2015. Brain amyloidosis and BDNF deficiency have opposite effects on brain volumes in AβPP/PS1 mice both in vivo and ex vivo. J. Alzheimers Dis. 46, 929–946.
Lau, J.C., Lerch, J.P., Sled, J.G., Henkelman, R.M., Evans, A.C., Bedell, B.J., 2008. Longitudinal neuroanatomical changes determined by deformation-based morphometry in a mouse model of Alzheimer's disease. NeuroImage 42, 19–27.
Lu, Y., Wu, X., Dong, Y., Xu, Z., Zhang, Y., Xie, Z., 2010. Anesthetic sevoflurane causes neurotoxicity differently in neonatal naïve and Alzheimer disease transgenic mice. Anesthesiology 112, 1404–1416.
Ma, Y., Hof, P.R., Grant, S.C., Blackband, S.J., Bennett, R., Slatest, L., McGuigan, M.D., Benveniste, H., 2005. A three-dimensional digital atlas database of the adult C57BL/6J mouse brain by magnetic resonance microscopy. Neuroscience 135, 1203–1215.
Manaye, K.F., Wang, P.C., O'Neil, J.N., Huang, S.Y., Xu, T., Lei, D.L., Tizabi, Y., Ottinger, M.A., Ingram, D.K., Mouton, P.R., 2007. Neuropathological quantification of dtg APP/PS1: neuroimaging, stereology, and biochemistry. Age (Dordr.) 29, 87–96.
Marjanska, M., Curran, G.L., Wengenack, T.M., Henry, P.G., Bliss, R.L., Poduslo, J.F., Jack Jr., C.R., Ugurbil, K., Garwood, M., 2005. Monitoring disease progression in transgenic mouse models of Alzheimer's disease with proton magnetic resonance spectroscopy. Proc. Natl. Acad. Sci. U. S. A. 102, 11906–11910.
Minkeviciene, R., Ihalainen, J., Malm, T., Matilainen, O., Keksa-Goldsteine, V., Goldsteins, G., Iivonen, H., Leguit, N., Glennon, J., Koistinaho, J., Banerjee, P., Tanila, H., 2008. Age-related decrease in stimulated glutamate release and vesicular glutamate transporters in APP/PS1 transgenic and wild-type mice. J. Neurochem. 105, 584–594.
Mlynárik, V., Cacquevel, M., Sun-Reimer, L., Janssens, S., Cudalbu, C., Lei, H., Schneider, B.L., Aebischer, P., Gruetter, R., 2012. Proton and phosphorus magnetic resonance spectroscopy of a mouse model of Alzheimer's disease. J. Alzheimers Dis. 31 (Suppl. 3), S87–S99.
Moffett, J.R., Ross, B., Arun, P., Madhavarao, C.N., Namboodiri, A.M., 2007. *N*-Acetylaspartate in the CNS: from neurodiagnostics to neurobiology. Prog. Neurobiol. 81, 89–131.
Naressi, A., Couturier, C., Devos, J.M., Janssen, M., Mangeat, C., de Beer, R., Graveron-Demilly, D., 2001. Java-based graphical user interface for the MRUI quantitation package. MAGMA 12, 141–152.
Park, M., Levine, H., Toborek, M., 2016. Exercise protects against methamphetamine-induced aberrant neurogenesis. Sci Rep 6, 34111.
Paslakis, G., Träber, F., Roberz, J., Block, W., Jessen, F., 2014. N-acetyl-aspartate (NAA) as a correlate of pharmacological treatment in psychiatric disorders: a systematic review. Eur. Neuropsychopharmacol. 24, 1659–1675.
Pijnappel, W.W.F., van den Boogaart, A., de Beer, R., van Ormondt, D., 1992. SVD-based quantification of magnetic resonance signals. J. Magn. Reson. 97, 122–134.
Price, J.L., Ko, A.I., Wade, M.J., Tsou, S.K., McKeel, D.W., Morris, J.C., 2001. Neuron number in the entorhinal cortex and CA1 in preclinical Alzheimer disease. Arch. Neurol. 58, 1395–1402.
Richner, M., Bach, G., West, M.J., 2009. Over expression of amyloid beta-protein reduces the number of neurons in the striatum of APPswe/PS1DeltaE9. Brain Res. 1266, 87–92.
Ross, B.D., Bluml, S., Cowan, R., Danielsen, E., Farrow, N., Tan, J., 1998. In vivo MR spectroscopy of human dementia. Neuroimaging Clin. N. Am. 8, 809–822.
Savonenko, A., Xu, G.M., Melnikova, T., Morton, J.L., Gonzales, V., Wong, M.P., Price, D.L., Tang, F., Markowska, A.L., Borchelt, D.R., 2005. Episodic-like memory deficits in the APPswe/PS1dE9 mouse model of Alzheimer's disease: relationships to beta-amyloid deposition and neurotransmitter abnormalities. Neurobiol. Dis. 18, 602–617.
Sawiak, S.J., Wood, N.I., Williams, G.B., Morton, A.J., Carpenter, T.A., 2009. Voxel-based morphometry in the R6/2 transgenic mouse reveals differences between genotypes not seen with manual 2D morphometry. Neurobiol. Dis. 33, 20–27.
Schuff, N., Amend, D., Ezekiel, F., Steinman, S.K., Tanabe, J., Norman, D., Jagust, W., Kramer, J.H., Mastrianni, J.A., Fein, G., Weiner, M.W., 1997. Changes of hippocampal *N*-acetyl aspartate and volume in Alzheimer's disease. A proton MR spectroscopic imaging and MRI study. Neurology 49, 1513–1521.
Skoog, I., Davidsson, P., Aevarsson, O., Vanderstichele, H., Vanmechelen, E., Blennow, K., 2003. Cerebrospinal fluid beta-amyloid 42 is reduced before the onset of sporadic dementia: a population-based study in 85-year-olds. Dement. Geriatr. Cogn. Disord. 15, 169–176.
Stefan, D., Di Cesare, F., Andrasescu, A., Popa, E., Lazariev, A., Vescovo, E., Strbak, O., Williams, S., Starcuk, Z., Cabanas, M., van Ormondt, D., Graveron-Demilly, D., 2010. Quantitation of magnetic resonance spectroscopy signals: the jMRUI software package. Meas. Sci. Technol. 20, 104035.
Sudduth, T.L., Greenstein, A., Wilcock, D.M., 2013. Intracranial injection of Gammagard, a human IVIg, modulates the inflammatory response of the brain and lowers Aβ in APP/PS1 mice along a different time course than anti-Aβ antibodies. J. Neurosci. 33, 9684–9692.
Teipel, S.J., Buchert, R., Thome, J., Hampel, H., Pahnke, J., 2011. Development of Alzheimer-disease neuroimaging-biomarkers using mouse models with amyloid-precursor protein-transgene expression. Prog. Neurobiol. 95, 547–556.
Tkác, I., Starcuk, Z., Choi, I.Y., Gruetter, R., 1999. In vivo 1H NMR spectroscopy of rat brain at 1 ms echo time. Magn. Reson. Med. 41, 649–656.